J. Fluid Mech. (1977), *vol.* 81, *part* 4, *pp.* 757–773
Printed in Great Britain

The formation of layers in a double-diffusive system with a sloping boundary

By P. F. LINDEN AND J. E. WEBER†
Department of Applied Mathematics and Theoretical Physics,
University of Cambridge

(Received 8 July 1976)

The flows induced by the presence of an insulating sloping boundary in a double-diffusive system are examined. In the diffusive case, when the component with the larger diffusivity is unstably distributed, it is known that under certain circumstances horizontal motions are induced near the slope, and that a series of horizontal layers forms. We investigate the formation and properties of the layers, in particular their vertical scale and its dependence on the stratification and the slope angle. The scale of the layers is found to be a strong function of $G\rho$, the ratio of the vertical density gradient of the unstably distributed component to that of the stably distributed component. At low values of $G\rho$, no layering was observed; at larger values of $G\rho$ layers were formed, and their scale increased as $G\rho \to 1$. A weak dependence of scale on slope angle was also observed with the scale diminishing as the angle of the slope to the horizontal increased.

A new form of layering has been observed when the basic stratification is in the finger sense. At high enough values of $G\rho$ the basic stratification is unstable to finger motions and these exist throughout the fluid. When a slope is introduced, horizontal motions are set up near the slope which cause the fingers to break down and layers are produced. There is considerable horizontal motion in these layers as well as convective motions driven by the fingers in the interfaces between the layers. The formation of these layers and some of their properties are documented.

1. Introduction

It is a remarkable fact that convective motion can be produced in a stably stratified fluid by the mere presence of an insulating sloping boundary. Working independently, Phillips (1970) and Wunsch (1970) showed that in a single-component stratification (where the density is a function of only one physical variable such as temperature) there is a flow induced up the sloping boundary which provides a convective flux of density to balance the flux produced by molecular diffusion in the interior of the fluid. It is easy to see how this flow arises. At an insulating boundary the isopycnals must be normal to the boundary. If the boundary is at an angle θ to the horizontal, where $0 < \theta < \frac{1}{2}\pi$, the isopycnals are bent from the horizontal at the wall. Vorticity is produced and a slope flow results. The flow is restricted to a thin buoyancy layer at the wall and is steady.

In this paper we examine the effects of a sloping boundary on a fluid which is stratified with two components which diffuse at different rates. Buoyancy-induced

† Present address: Institute of Mathematics, Mechanics Department, University of Oslo.

motions which occur in fluids stratified in this way are known as double-diffusive flows. When one of the components is unstably distributed in the fluid, the energy stored in the distribution of this component can, in certain circumstances, be released and drive a wide variety of convective flows. Double-diffusive flows occur in a wide range of situations, in oceanography, chemical engineering and astrophysics. The interaction of such flows with topography and other forms of non-uniform geometry is likely to be important in these contexts. Furthermore, the role of horizontal non-uniformities in the components driving the convection is an important but still largely unknown quantity, and the presence of a sloping boundary provides a convenient way of examining some of its properties.

There are two classes of double-diffusive convection depending on which component is unstably stratified. If it is the slower diffusing component, the convection typically takes the form of long vertical cells and this class is called 'finger' convection. On the other hand, if the faster diffusing component is unstably stratified, the motion is called 'diffusive'. The detailed characteristics of these two types of flow can be quite different and the reader is referred to Turner (1973, chap. 8) for a general discussion of their properties.

The effects of a sloping boundary on a double-diffusive system stratified in the diffusive sense have been examined by Turner (1973), Turner & Chen (1974) and Chen & Wong (1974). They found that, even though the basic stratification was statically stable (density increased downwards), the initial flow was down the slope in contrast to the one-component case. They also observed that advection by this slope flow reversed the local vertical gradients and fingers were formed near the boundary. Eventually this motion was found to break down into a series of horizontal layers which propagated away from the slope.

Here we investigate this layer formation over a range of slope angles and density gradients. We also examine the flows induced when the basic stratification is in the finger sense. We begin our discussion by looking at some theoretical aspects of the flow produced by a sloping boundary in § 2. In § 3 the experimental methods used to investigate these motions are explained and the results given in § 4. A comparison of the theory and experiments is given in § 5, and some conclusions are drawn in § 6.

2. Basic flow: asymptotic solutions

Consider a fluid stratified with two components T and S with coefficients of molecular diffusion κ_T and κ_S, respectively. For definiteness we take $\tau \equiv \kappa_S/\kappa_T$ such that $0 < \tau < 1$. We suppose that in the undisturbed case the vertical density gradient produced by each component is separately constant, so that we can write the density distribution as

$$\rho = \rho_0(1 + \gamma_T z + T + \gamma_S z + S). \tag{2.1}$$

Here ρ_0 is a mean density, $\rho_0 \gamma_{T,S}$ is the initial density gradient due to T, S, and T and S are perturbations about this initial state. These deviations from the initial state are brought about by an insulating sloping boundary at an angle θ to the horizontal introduced at time $t = 0$. We also assume that the fluid is infinite in vertical and horizontal extent, except for the presence of the slope, and that the slope is infinite in the y direction (see figure 1).

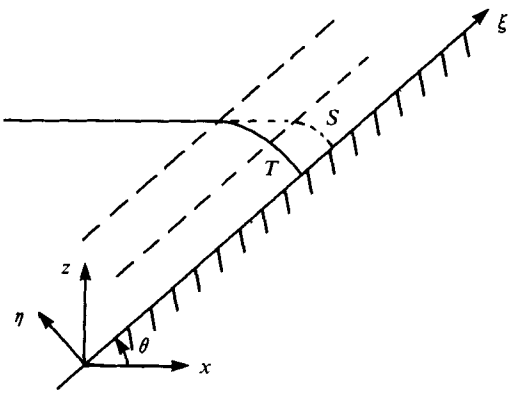

FIGURE 1. A definition sketch showing the relation of the co-ordinate axes to the slope. The initial diffusion-induced downward distortions of the isopleths of T and S are also shown.

We impose the condition that the flow be stably stratified, i.e. $\gamma_T+\gamma_S<0$, and we look for flows which are independent of the co-ordinate along the slope ξ. The equations governing such motions are

$$u_t = \nu u_{\eta\eta} - g\sin\theta\,(T+S), \tag{2.2}$$

$$T_t = \kappa_T T_{\eta\eta} - \gamma_T \sin\theta\, u, \tag{2.3}$$

$$S_t = \kappa_S S_{\eta\eta} - \gamma_S \sin\theta\, u, \tag{2.4}$$

where ν is the coefficient of kinematic viscosity and subscripts represent partial differentiation. The boundary conditions are

$$u=0, \quad T_\eta = -\gamma_T\cos\theta, \quad S_\eta = -\gamma_S\cos\theta \quad \text{on} \quad \eta=0, \tag{2.5}$$

$$u, T, S \to 0 \quad \text{as} \quad \eta\to\infty. \tag{2.6}$$

It is a simple matter to show that (2.2)–(2.4) have no steady-state solutions which satisfy all the boundary conditions. Assuming $\partial/\partial t = 0$, we readily obtain a solution which vanishes at infinity, namely

$$\left.\begin{aligned} u &= A\,e^{-M\eta}\sin M\eta, \\ T = \frac{A\gamma_T\sin\theta}{2\kappa_T M^2}e^{-M\eta}\cos M\eta, \quad S &= \frac{A\gamma_S\sin\theta}{2\kappa_S M^2}e^{-M\eta}\cos M\eta, \end{aligned}\right\} \tag{2.7}$$

where

$$M^4 = -\left(\frac{\gamma_T}{\kappa_T}+\frac{\gamma_S}{\kappa_S}\right)\frac{g\sin^2\theta}{4\nu}. \tag{2.8}$$

The wall boundary conditions (2.5) on T and S finally imply

$$A = 2M\kappa_T\cos\theta, \quad A = 2M\kappa_S\cos\theta,$$

which are inconsistent unless $\kappa_T=\kappa_S$. Hence there is no steady-state solution for $\tau\neq 1$.

It is instructive to examine the physical cause of this behaviour. If the fluid is not semi-infinite in the η direction but is confined to a slot between parallel sloping walls a finite distance apart, a steady-state solution can be found (Chen 1975). This steady state is achieved by distorting the isopleths of T and S right across the slot. In the

semi-infinite case there is always a region far enough from the slope where the original gradients of T and S are undisturbed and where the original diffusive vertical fluxes exist. In the one-component case Phillips (1970) showed that a steady state was achieved even in a semi-infinite fluid by balancing the vertical diffusive flux in the interior by the vertical component of a convective flow along the slope. In the two-component case this balance can never be achieved by a single flow as it is necessary to balance two interior fluxes. Not only does this preclude a steady state but it also means that horizontal differences in T, S and density will develop in the fluid which can make the slope flow unstable. It is these instabilities which we shall examine experimentally, but before doing so, we shall consider the unsteady slope flow in a little more detail.

We solve (2.2)–(2.4) asymptotically for small and large times, by taking the appropriate limits of the Laplace transform of these equations. The solution for small times, which is just the initial diffusive response to the no-flux condition at the wall, is

$$u = -\frac{4g\sin 2\theta\gamma_S(\kappa_T t)^{\frac{3}{2}}}{\nu}\left\{\frac{\lambda}{1-\sigma^{-1}}\mathrm{i}^3\operatorname{erfc}\frac{\eta}{2(\kappa_T t)^{\frac{1}{2}}} - \frac{\tau^{\frac{1}{2}}}{\tau^{-1}-\sigma^{-1}}\mathrm{i}^3\operatorname{erfc}\frac{\eta}{2(\kappa_S t)^{\frac{1}{2}}}\right.$$
$$\left. + \left(\frac{\tau^{\frac{1}{2}}}{\tau^{-1}-\sigma^{-1}} - \frac{\lambda}{1-\sigma^{-1}}\right)\mathrm{i}^3\operatorname{erfc}\frac{\eta}{2(\nu t)^{\frac{1}{2}}}\right\}(1+O(\gamma_S^2\kappa_S t)), \quad (2.9)$$

$$T = 2\cos\theta\gamma_T(\kappa_T t)^{\frac{1}{2}}\,\mathrm{i}\operatorname{erfc}\frac{\eta}{2(\kappa_T t)^{\frac{1}{2}}}(1+O(\gamma_S^2\kappa_S t)), \quad (2.10)$$

$$S = 2\cos\theta\gamma_S(\kappa_S t)^{\frac{1}{2}}\,\mathrm{i}\operatorname{erfc}\frac{\eta}{2(\kappa_S t)^{\frac{1}{2}}}(1+O(\gamma_S^2\kappa_S t)), \quad (2.11)$$

where $\lambda = -\gamma_T/\gamma_S$, $\sigma = \nu/\kappa_T$ and $\mathrm{i}^n\operatorname{erfc}$ represents the nth repeated integral of the complementary error function. The solutions for $T+\gamma_T z$ and $S+\gamma_S z$ are sketched on figure 1. The horizontal isopleths bend down to meet the slope at right angles, the bending occurring in diffusive boundary layers of thickness $\delta_T \sim (\kappa_T t)^{\frac{1}{2}}$ and $\delta_S \sim (\kappa_S t)^{\frac{1}{2}}$. This distortion sets up a horizontal density gradient, which generates vorticity, resulting in the slope flow u given by (2.9).

The direction of this initial flow depends on the details of the stratification. For example, suppose the basic stratification is diffusive (i.e. $\gamma_T > 0$, $\gamma_S < 0$). Then the downward distortion of T near the wall increases the density there, which is offset by a reduction due to distortion of the S field. Depending on the relative magnitudes of γ_T and γ_S we see that it is possible to have either upflows or downflows near the slope. Quantitatively, a series development of (2.9) for small η shows that the flow near the slope is down when $\lambda > F$ and up when $\lambda < F$, where

$$F = \tau(\sigma-1)(\sigma^{\frac{1}{2}}-\tau^{\frac{1}{2}})/(\sigma^{\frac{1}{2}}-1)(\sigma-\tau). \quad (2.12)$$

As $\sigma\to\infty$, $F\to\tau$, while for σ finite and $\tau\to 0$, $F\to(\sigma-1)\tau/(\sigma-\sigma^{\frac{1}{2}})$. For sugar and salt in water $F = 0{\cdot}34$. On the other hand, if the basic stratification is finger like, a series development shows that the flow is always up the slope. This is easily seen from figure 1, as $|\gamma_T| > |\gamma_S|$ and so the greater distortion of the T field ensures that the net density decreases near the wall compared with the undisturbed density at that level.

The solution for large times is given by

$$u = 2\cot\theta\frac{\tau(1-\lambda)}{1-\tau\lambda}\kappa_T M\, e^{-M\eta}\sin M\eta(1+O(g\gamma_S t^2)^{-\frac{1}{4}}), \tag{2.13}$$

$$T = \gamma_T\cos\theta\left\{\frac{\tau(1-\lambda)}{1-\tau\lambda}M^{-1}e^{-M\eta}\cos M\eta + \frac{2(1-\tau)(\kappa_T t)^{\frac{1}{2}}}{[(1-\lambda)(1-\tau\lambda)]^{\frac{1}{2}}} \times \mathrm{i}\,\mathrm{erfc}\left[\left(\frac{1-\lambda}{1-\tau\lambda}\right)^{\frac{1}{2}}\frac{\eta}{2(\kappa_T t)^{\frac{1}{2}}}\right]\right\}(1+O(g\gamma_S t^2)^{-\frac{1}{4}}), \tag{2.14}$$

$$S = \gamma_S\cos\theta\left\{\frac{1-\lambda}{1-\tau\lambda}M^{-1}e^{-M\eta}\cos M\eta + \frac{2\lambda(1-\tau)(\kappa_T t)^{\frac{1}{2}}}{[(1-\lambda)(1-\tau\lambda)]^{\frac{1}{2}}} \times \mathrm{i}\,\mathrm{erfc}\left[\left(\frac{1-\lambda}{1-\tau\lambda}\right)^{\frac{1}{2}}\frac{\eta}{2(\kappa_T t)^{\frac{1}{2}}}\right]\right\}(1+O(g\gamma_S t^2)^{-\frac{1}{4}}), \tag{2.15}$$

where M is defined by (2.8). This solution is valid for all λ in the diffusive case ($\lambda < 1$), and for $\lambda > \tau^{-1}$ in the finger case. For $1 < \lambda < \tau^{-1}$ the solution is invalid, but in this case the basic stratification is unstable to infinitesimal disturbances of the finger type (see Turner 1973), and so the basic state described by (2.1) does not exist.

The large time solution (2.13)–(2.15) consists of two parts. One is a stationary buoyancy-layer type of solution analogous to the one-component case. Since a single flow cannot balance two interior diffusive fluxes, the solution will always contain a transient part. It is worth noting, however, that the generation of vorticity due to the transient T and S parts tends to vanish outside the buoyancy layer, such that the flow is confined to this boundary region. The typical layer thickness is M^{-1}, and the flow is, in all cases, up the slope. In the limit $\tau = 1$, $\lambda = 0$, we reduce to the one-component stratification, and the large time solution reduces to the steady-state solution found by Phillips (1970). For the diffusive stratification for $\lambda > F$ we see that the flow is initially down the slope and then must reverse at some later time in order to reach the final state described by (2.13). This reversal in the direction of motion was also found in a tilted slot by Chen (1975).

There is one other class of flows which is related to those described here. It occurs when a stable solute gradient (e.g. salt) is heated at a side boundary. There is upflow near the heated boundary and this flow distorts the isohalines near the wall. For sufficiently large Rayleigh numbers (i.e. side-wall temperatures) this basic flow becomes unstable owing to the fact that $\kappa_T \neq \kappa_S$, and a motion develops which takes the form of horizontal layers intruding into the interior. The linear stability of this system has been studied by Thorpe, Hutt & Soulsby (1969) and the finite amplitude motions by Chen, Briggs & Wirtz (1971).

In the heated side wall experiments of Chen *et al.* (1971) the vertical scale of the layers which form is of the order of $\Delta T/(dS/dz)$, where ΔT is the horizontal temperature difference imposed at the wall and dS/dz the interior salinity gradient, both in density units. The similarity with the sloping boundary experiments arises from the fact that the presence of an insulating slope is equivalent to applying a constant horizontal flux of T and S to the system (see the appendix).

3. The experimental method

The experimental techniques used to examine the flows induced in a two-component stratified fluid are standard and so only a brief description of them will be given here. In all the experiments sugar and salt were used as the two diffusing components. In the notation of § 2, salt is the faster diffusing component, denoted by T, and sugar the slower diffusing component S: $\kappa_S = 0{\cdot}5 \times 10^{-5}\,\mathrm{cm^2\,s^{-1}}$, $\kappa_T = 1{\cdot}5 \times 10^{-5}\,\mathrm{cm^2\,s^{-1}}$ and $\tau = \kappa_S/\kappa_T = 0{\cdot}33$.

The experiments were carried out in a rectangular Perspex tank of length 91·5 cm, width 7·6 cm and depth 30·5 cm. The tank was filled to a depth of about 25 cm with uniform opposing gradients of sugar and salt using a 'double-bucket' filling technique (Oster 1965). It took about 1–2 hours to fill the tank. The solutions were allowed to stand after preparation until they had reached room temperature. The density of each solution was in the range 0·998–1·010 $\mathrm{g\,ml^{-1}}$, and was measured with a hydrometer accurate to 0·5‰.

Two forms of sugar–salt stratification were used: in the diffusive case the saccharinity decreased whilst the salinity increased with height, and vice versa for the finger case. Two parameters are required to specify the stratification in each case. We shall use $N = (-g\rho_0^{-1}\,d\rho/dz)^{\frac{1}{2}}$, the buoyancy frequency of the density gradient, and $G\rho$, the ratio of the density gradients of the two components. This means in the notation of § 2 that for the diffusive case $G\rho = |\lambda|$, whilst for the finger case $G\rho = |\lambda|^{-1}$. Defined in this way $0 < G\rho < 1$, the upper limit being attained when the two components contribute equally to the density gradient and $N = 0$. In the case $G\rho = 0$ there is no unstable component and double-diffusive effects are absent. Situations where $G\rho > 1$ correspond to the density increasing with height and are excluded from the discussion. Therefore the magnitude of $G\rho$ gives an indication of the relative importance of double-diffusive effects, and the similarities which will emerge between the finger and diffusive cases are most readily brought out by the use of $G\rho$ in this way. Any ambiguities which may arise from the use of one symbol for two situations should be resolved by the immediate context of its use.

Implicit in the above method of producing constant vertical gradients of the various components is the requirement that the cross-sectional area of the tank be uniform with height. The presence of a single sloping wall will violate this condition. In order to overcome this difficulty two methods of introducing a sloping boundary into the fluid were used. In the first, the tank was filled and subsequently a slope was introduced by sliding a metal plate down between two slots milled in the side walls of the tank (see figure 3, plate 1). The slots were at 45° to the horizontal and so to examine the effects of slopes at other angles a second method was used. A metal plate slightly smaller than the width of the tank was inserted at the required angle and held in place by a small wedge. Thus, over most of the depth there was a small (0·5 cm) gap between the slope and one of the side walls of the tank, and the tank could now be filled in the usual manner. By comparing the two methods we were able to confirm the conjecture made by Turner & Chen (1974) that the disturbances produced when the slope was inserted after filling had little effect on the flow which subsequently developed.

Unfortunately, it was possible to fill the tank with the slope in position only for the diffusive case. In order to get a horizontally uniform finger stratification it was necessary to add fluid evenly along the full length of the tank. This was achieved by

using three floats which covered the water surface and by supplying each of them with fluid independently. So for the finger case the slope was always inserted once the tank was full and only one angle ($\theta = \frac{1}{4}\pi$) was used.

A shadowgraph was used, in conjunction with observations of the distortions of dye traces, to visualize the flows. Both still and time-lapse ciné photography were used to record the motions. Photographs of the dye traces at subsequent times, which were recorded by a digital clock accurate to 0·1 s, gave quantitative information about the velocity fields, while many of the qualitative observations come from viewing the time-lapse movies.

Before describing the results in detail it is appropriate to say a little about the interpretation of the data and the errors involved in the measurements. The experiments consisted of setting up the initial stratification and then watching the motion which developed as it interacted with the slope. Each experiment was essentially transient as there was no mechanism for maintaining the initial vertical gradients (even in the mean). Therefore recognition of the different phases of an experiment and comparison of different experiments in the same phase is a somewhat subjective process. Furthermore, many of the motions observed appear to be turbulent. Consequently, the errors involved in the actual measurements, such as parallax in the photographs of the dye traces, inaccuracies in reading the hydrometers and so on, are normally negligible when compared with the more serious, and less easily quantifiable, uncertainties resulting from the transient and turbulent nature of the flows. This is not to say that it is impossible to be quantitative and we have put error bars on the data wherever appropriate, but these difficulties in interpretation should be borne in mind. Some further discussion of the variability of the motions will be given when the results are presented.

4. The experimental results

Diffusive stratification

The flow induced in a diffusive stratification by a sloping boundary is a strong function of the ratio of the interior density gradients $G\rho$. At low values of $G\rho$ (the meaning of low in this context will be quantified later) there was almost no observable motion, but in some cases very weak layers formed immediately adjacent to the slope. An example of this weak layering is shown on figure 2 (plate 1). In this case $G\rho = 0{\cdot}87$ and $\theta = \frac{1}{4}\pi$. The layers, having a typical vertical scale of about 0·4 cm, appeared to form spontaneously along the length of the plate and they remained unchanged for a day or so until they were destroyed by layers growing down from the top of the tank. These larger-scale layers appear to result from evaporation at the free surface and are not related to the presence of the slope: some of them can be seen at the top of the fluid.

At high values of $G\rho$ the sequence of events is much different. Consider for the moment the upper side of the slope (i.e. the left-hand side of the photographs). The initial response is for a downflow to develop near the slope. This reverses the local vertical gradients of T and S near the wall and fingers are produced locally. These fingers, which transport dense fluid downwards, advect heavy fluid onto the slope and reinforce the downflow. Evidence of this downflow and the fingers can be seen on figure 3 (plate 1). Although not directly obvious from a still photograph, the effects

of the downflow can be seen by the presence of structure beneath the end of the slope. This structure was produced by dense fluid running down and off the end of the slope. On the underside of the slope the flow is upwards, and again the local T and S gradients are reversed and fingers form. Dye deposited on the upper side of the slope was advected down the slope and then advected upwards on the underside as can be seen on figure 3.

The next stage in the process is the breakdown of this slope flow and the formation of horizontal layers. The beginnings of this can be seen by the horizontal advection of the dye in figure 3. A more advanced stage of the layer formation is shown on figure 4 (plate 2). The slope flow has ceased on the top of the upper side of the plate but still exists further down. The vertical transport from the slope by the fingers near the bottom can be seen from the spreading of the dye. On the underside of the slope layers have formed near the bottom but the slope flow and fingers persist at the top. The layers have the characteristic form found by Turner & Chen (1974) of a very sharp diffusive interface on one side and a finger interface on the other. At the ends of the layers there are often, but not always, well defined 'noses'. These propagate across the tank until they reach an end wall. The distortion of the vertical dye streaks shows the large shears ($0{\cdot}1\ \mathrm{s}^{-1}$) across the interface, and the streak on the right shows that disturbances propagate ahead of the advancing layers.

Figure 5 (plate 2) shows two later stages of a similar experiment. In figure 5(*a*), although a large number of layers have formed, the system is still very active with typical velocities of around $0{\cdot}02\ \mathrm{cm\,s}^{-1}$. Vigorous convection is taking place in the layer and several of the interfaces are exhibiting signs of breaking down in a manner very reminiscent of that found in other diffusive situations (see Linden 1976). There is still considerable shear across the interfaces and once the layer has reached the end wall of the tank the motion is such that the circulation is in the same sense as the original slope flow, giving clockwise circulation on both sides of the slope. At a much later time the irregularities in the layers disappear and we are left with a regular structure as can be seen on figure 5(*b*). This set of layers persisted for several days with the interfaces eventually becoming weaker as a result of molecular diffusion.

These two examples of the different types of layering are typical of all the experiments, with two exceptions. At even lower values of $G\rho < 0{\cdot}7$ no layering was observed at all. In some cases, particularly for other slope angles, an intermediate form was observed. A weak slope flow induced weak fingers which eventually died out without producing the active layers shown on figures 3, 4 and 5. This intermediate case appeared to represent the transition from low-$G\rho$ to high-$G\rho$ systems and did not reveal any new features.

The most obvious difference between low-$G\rho$ layers (figure 2) and high-$G\rho$ layers (figure 5) is their scale. Both the vertical and the horizontal scale of the layers is greater in the high-$G\rho$ case. On figure 6 we show the mean vertical scale $\bar{h}$ of the layers plotted against $1 - G\rho$ for a fixed slope angle $\theta = \frac{1}{4}\pi$. We plot the data in this way in order to emphasize the fact that we need $G\rho > 0{\cdot}7$ to get layers at all. The determination of $\bar{h}$ depends on what stage of the formation process is considered and we have chosen the one corresponding to figure 5(*b*). Before this time there are irregular and incomplete layers which make $\bar{h}$ a function of horizontal position. Later, there is a gradual increase in scale as some layers merge, but this occurs on a much longer time scale, typically several hours.

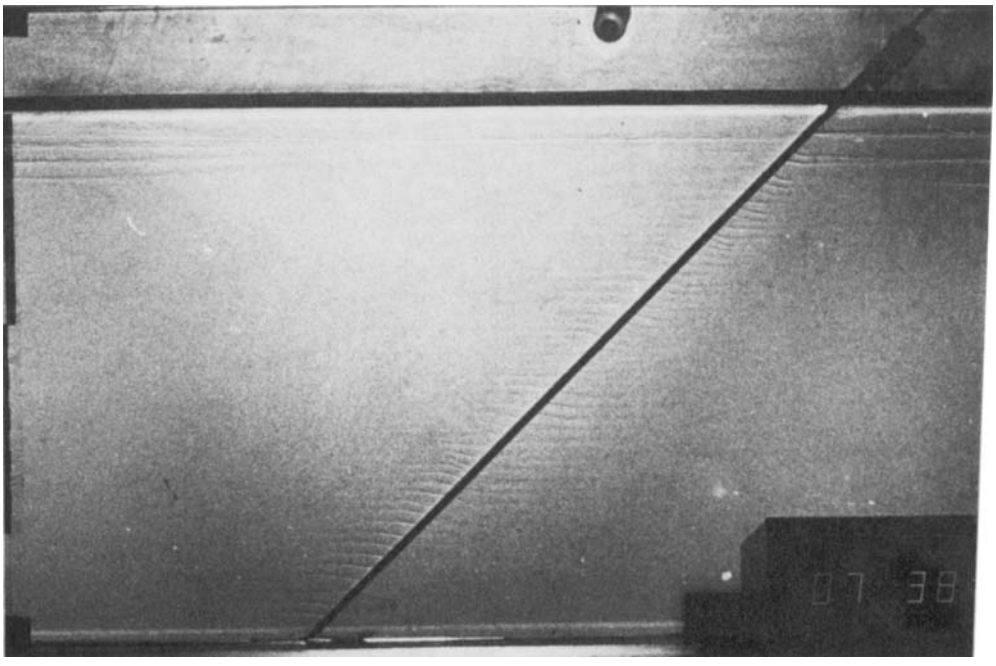

FIGURE 2. Layers observed for a diffusive stratification with $N = 0{\cdot}66$ rad/s, $G\rho = 0{\cdot}87$ and $\theta = \frac{1}{4}\pi$. In this run the tank was filled with the slope fixed in position (held by the wedge visible above the surface). In the lower right corner can be seen the time in hours and minutes since the filling of the tank began. The tape on the left-hand side is offset in 10 cm lengths.

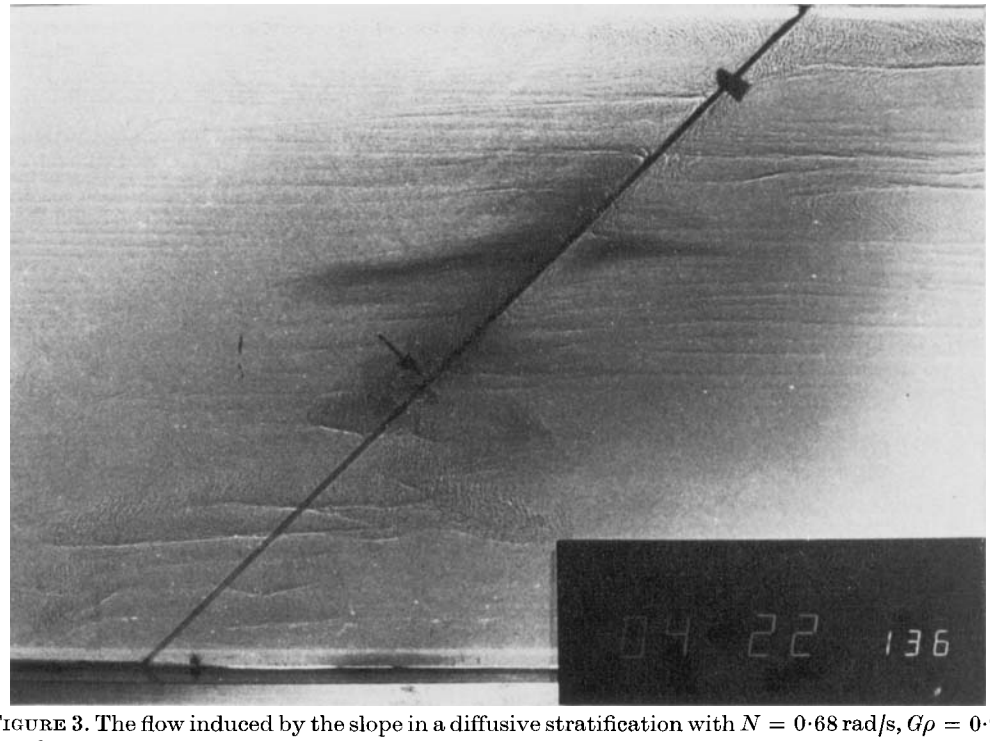

FIGURE 3. The flow induced by the slope in a diffusive stratification with $N = 0{\cdot}68$ rad/s, $G\rho = 0{\cdot}90$ and $\theta = \frac{1}{4}\pi$. In this case the slope was inserted only part of the way into the tank. The slope can be identified by the dark line on the shadowgraph and its end is marked by an arrow, and the slots into which it is fitted are visible in the lower part of the photograph. The clock in this case records the hours, minutes, seconds and tenths since the filling began.

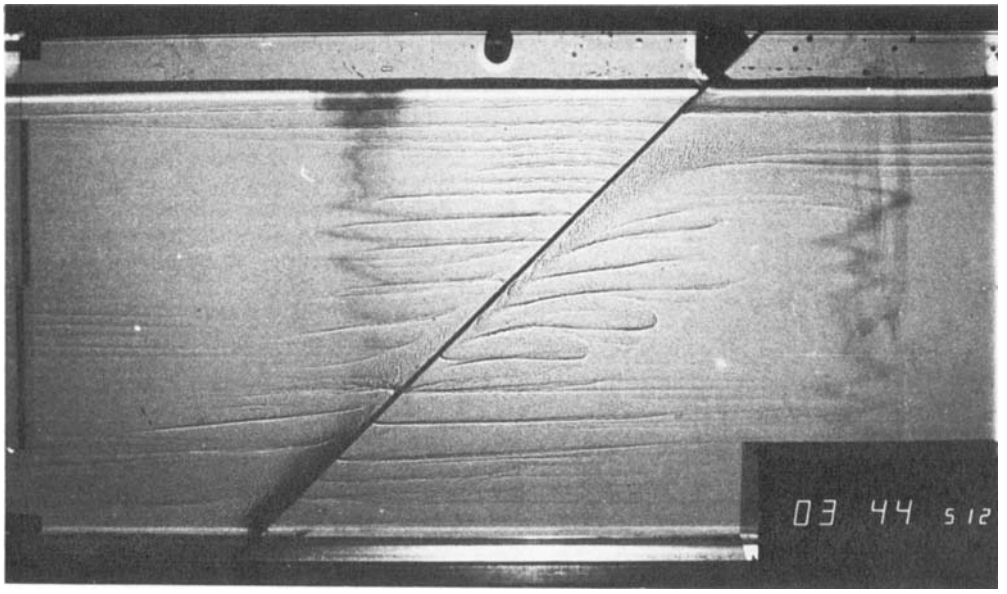

FIGURE 4. An intermediate stage in the layer formation in a diffusive stratification with $N = 0{\cdot}60$ rad/s, $G\rho = 0{\cdot}89$ and $\theta = \frac{1}{4}\pi$. The tank was filled before the slope was inserted. The time on the clock registers the elapsed time since the slope was introduced. The tape on the left-hand side is offset in 10 cm lengths.

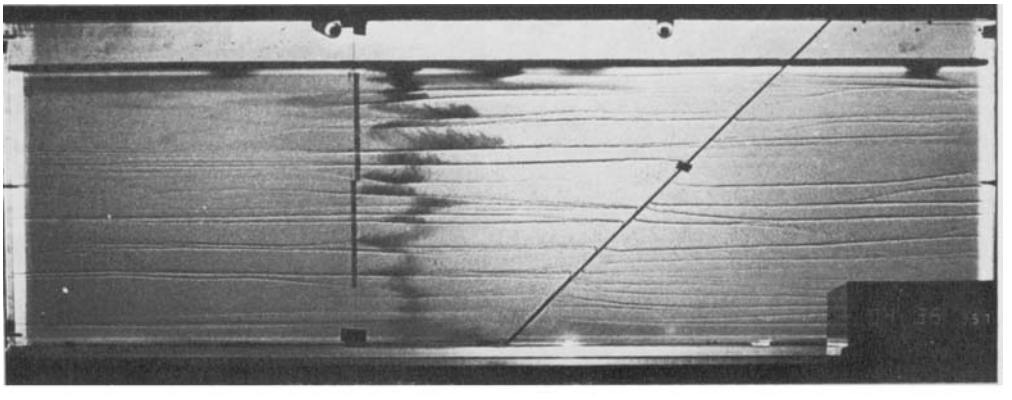

(*a*)

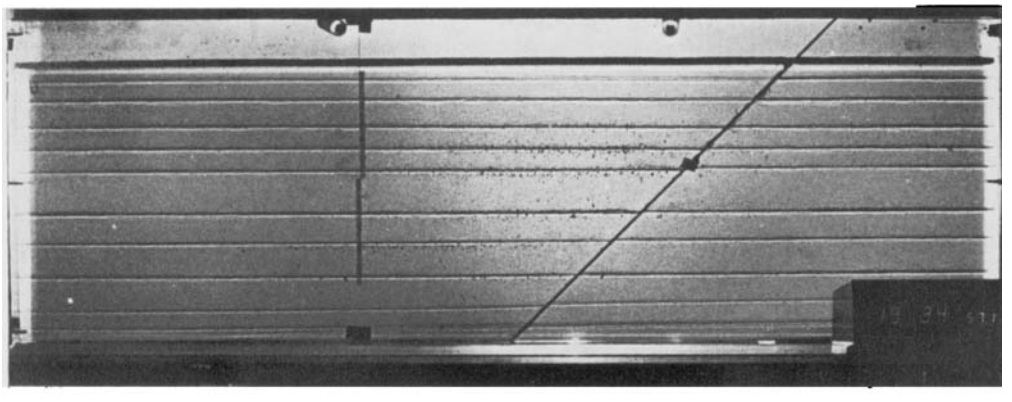

(*b*)

FIGURE 5. For legend see facing page.

We see that there is a rapid increase in scale as $G\rho \to 1$, a phenomenon which has been observed in other configurations (Linden 1976). Unfortunately, owing to the inherent instability of the basic stratification as $G\rho \to 1$, the maximum value which could be attained was $G\rho = 0{\cdot}95$. For values of $G\rho < 0{\cdot}95$ there was no evidence of instability provided the sloping boundary was not introduced. In the range

$$0{\cdot}89 < G\rho < 0{\cdot}95$$

fingers were observed once the slope was introduced, whilst for $G\rho < 0{\cdot}87$ the layers formed in the absence of fingers as shown in figure 2.

The effect of variation in the slope angle θ is shown on figure 7, which is a plot of $\bar{h}$ against θ for a fixed value of the gradient ratio $G\rho = 0{\cdot}9$. From this figure we see that the presence or absence of fingers depends on θ as well as on $G\rho$, with the most vigorous finger activity occurring for $\frac{1}{9}\pi < \theta < \pi/3{\cdot}6$. The scale of the layers decreases as θ increases with no layers observed for $\theta > \frac{1}{3}\pi$. At very low slope angles ($\theta < \frac{1}{36}\pi$) layers are not formed. This is due to the fact that the advection terms tend to vanish in this limit; see (2.2)–(2.4). We also note that the terminology of low-$G\rho$ and high-$G\rho$ stratifications used above is appropriate only for a fixed angle.

The variation in the horizontal scale of the layers is much more difficult to quantify. In the weak layering case the layers do not extend very far from the slope (figure 2) and their length is not easily determined. In the strong layering case the layers always extended to the end walls of the tank. This large horizontal extent in the latter case seems to be connected with the presence of the noses at the front of the extending layers. Turner & Chen (1974) mention that in some cases the noses appear to propagate independently of the slope flow and can apparently convert the potential energy stored in the diffusive stratification into kinetic energy to drive their own motions. We also observed this phenomenon and feel that the noses are in themselves sufficiently interesting for us to document some of their properties here.

The form of the noses varies from the relatively smooth type shown on figure 4 to the more turbulent structures, an example of which is given on figure 8 (plate 3). In each case the front of the nose is quite sharply defined on the shadowgraph, and appears to be two-dimensional, even though the motion inside the nose is quite vigorous. Of the two interfaces associated with the nose one is diffusive and relatively sharp whilst the other contains fingers and can be rather poorly defined. There is motion inside the nose driven, at least in part, by the convective fluxes across these interfaces. The speed of this interior circulation is considerably greater than the propagation velocity of the nose U, varying from about 2–5 times U.

The horizontal displacements of some typical noses are plotted against time on

---

LEGEND TO FIGURE 5

FIGURE 5. The final stages in the production of a set of layers for the diffusive stratification $N = 0{\cdot}48$ rad/s, $G\rho = 0{\cdot}95$ and $\theta = \frac{1}{4}\pi$. The tank was filled with the slope in position and the clock records the time since the filling began. The specks concentrated near some of the interfaces in (*b*) are the residue of the dye introduced in (*a*). In (*b*) it is seen that the interfaces are at exactly the same depths on either side of the slope. This is a result of the fact that the small gap on one side of the slope, which occurs when the slope is fixed in position before the tank is filled, allows the motions on each side to be influenced by those on the other. This influence does not affect the early stage of the layer formation (see (*a*)) but does lead to the symmetry at much larger times.

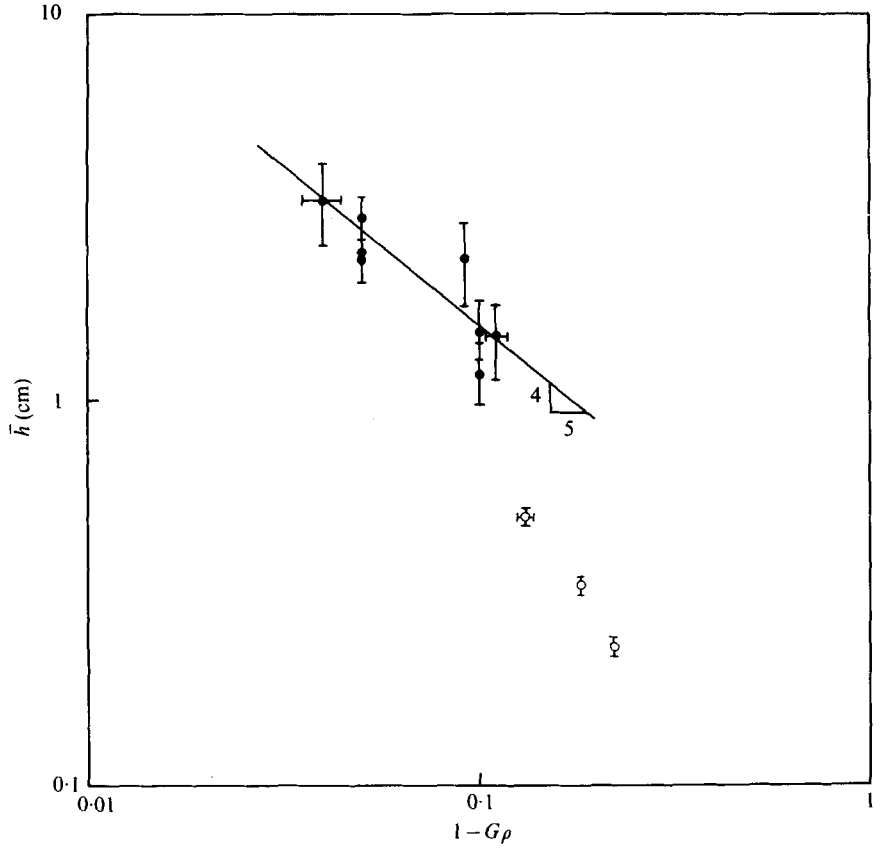

FIGURE 6. A log–log plot of the mean vertical scale of the layers $\bar{h}$ (cm) against $1-G\rho$ for a fixed angle $\theta = \frac{1}{4}\pi$. The closed circles imply runs where fingers were observed and open circles runs where no fingers were observed. The error bars represent two standard deviations about the mean of $\bar{h}$. The solid line is a line of slope $-0{\cdot}8$.

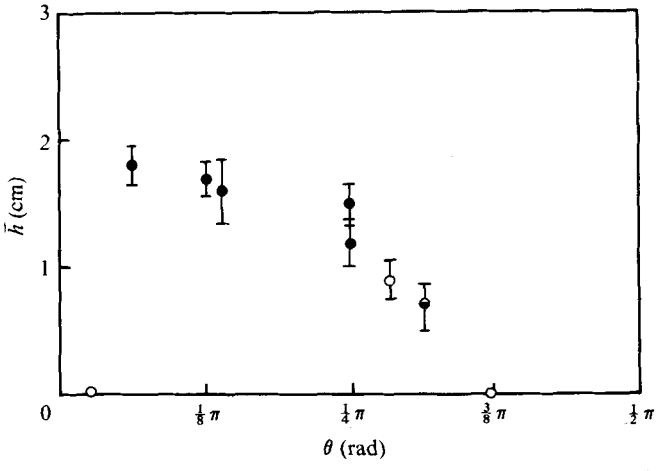

FIGURE 7. The mean vertical scale of the layers $\bar{h}$ (cm) plotted against the slope angle θ, for fixed $G\rho = 0{\cdot}90$. The symbols have the same meaning as on figure 6, except for the half-closed circles, which indicate the transition from strong-finger to no-finger slope flows.

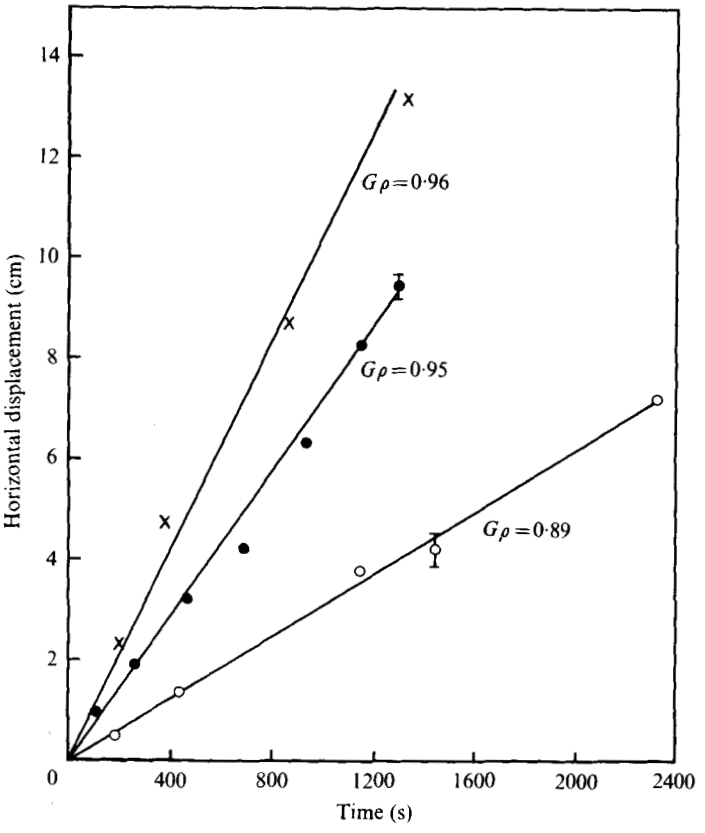

FIGURE 9. The horizontal displacement of a nose plotted against time. Three different values of $G\rho$ of the basic stratification are shown. The straight lines are fitted through the points by eye.

figure 9. We see that to a good approximation the horizontal velocity is constant. The motion of a nose is not completely horizontal as the mean density inside the nose changes with time owing to the fluxes across the interfaces. However, the vertical motion is quite small compared with the horizontal displacement. Figure 10 shows the horizontal velocity of the nose U, non-dimensionalized by the depth of the layer behind the nose h and the buoyancy frequency N of the stratification, plotted against the ratio of the density gradients $G\rho$. There is a considerable amount of scatter in the data but two facts emerge. First, the non-dimensional velocity increases as $G\rho$ approaches unity, and second, $U/Nh \sim 5 \times 10^{-3}$ in order of magnitude. We shall comment further on these results in § 5.

Finger stratification

All but one of the experiments carried out with finger stratification had supercritical density ratios $G\rho > \tau$. (The exception was one case run with $G\rho = 0{\cdot}29$; none of the motions described below were observed in this case and we shall consider it no further.) This meant that the basic stratification was unstable to finger motions and fingers were present throughout the tank before the slope was inserted. Another implication of the supercritical nature of the basic stratification is that none of the analysis described in § 2 applies to these situations.

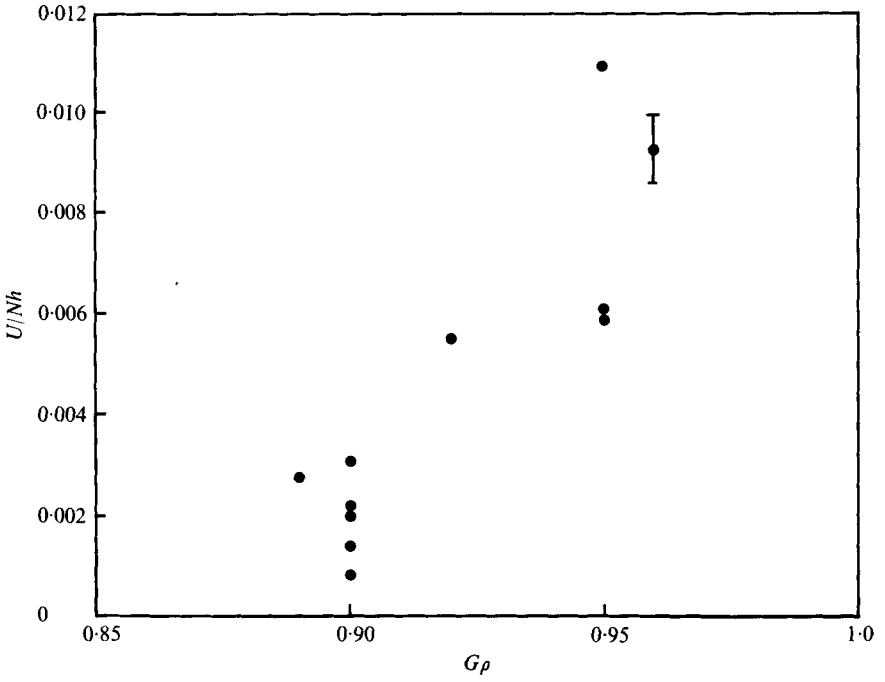

FIGURE 10. The horizontal velocity of the nose U non-dimensionalized with respect to the buoyancy frequency N and the thickness h of the layer behind the nose plotted against the gradient density ratio $G\rho$. The values of U are determined from the slope of displacement *vs.* time plots such as those shown on figure 9. The length of the error bars reflects the extreme values of U/Nh which could be reasonably achieved by fitting a different line through the points or owing to variations in h. Note that values of $G\rho$ start at 0·85.

An example of the motions produced by the slope is shown on figure 11 (plate 3). This photograph, taken nearly 79 min after the slope was inserted into a uniform field of fingers with $G\rho = 0{\cdot}91$, shows a number of horizontal layers separated by interfaces containing fingers. The sequence of events leading up to the formation of these layers is as follows. The downward advection of dense fluid by the fingers leads to an accumulation of this dense fluid on the upper side of the slope and a downslope flow develops. Evidence of this slope flow can be seen in figure 11 from the dye which was added about half way down the slope. This dye has been advected down the slope and has collected in a pool at the bottom. The dye can also be seen to have been advected vertically by the fingers above the lower half of the slope. On the underside of the slope advection of less dense fluid upwards by the fingers causes an upslope flow there.

During this stage there is also a weakening of the fingers at the top of the upper side of the slope and beneath the slope in the corner near the bottom of the tank. This weakening appears to result from the fact that the presence of the slope cuts off the supply of sugar and salt to the fingers in these corner regions. This reduction in intensity was observed first in the corners and then spread slowly outwards with increasing time. This feature can be seen from the lack of small-scale vertical structure in these corner regions on figure 11.

The layers were first noticeable in this particular case about 40 min after the slope was inserted. At this time some horizontal distortion of the fingers near the slope

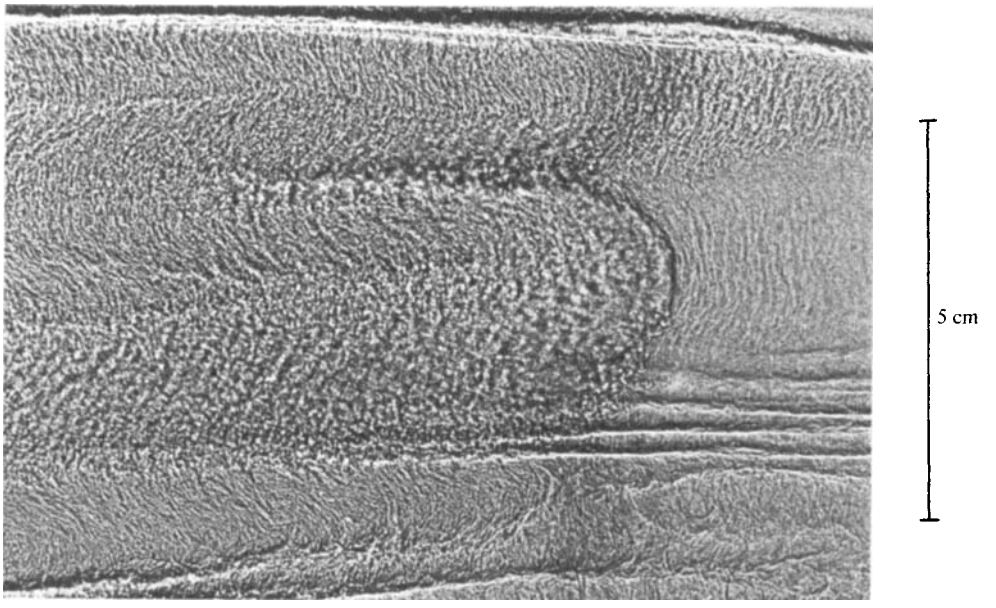

FIGURE 8. A close-up of a turbulent nose in a diffusive stratification with $G\rho = 0{\cdot}95$. The nose is propagating from left to right. At this high value of $G\rho$ the distinction between the two kinds of interface seen behind the noses shown on figure 4 is not as clear, owing to the very turbulent motion in the nose itself.

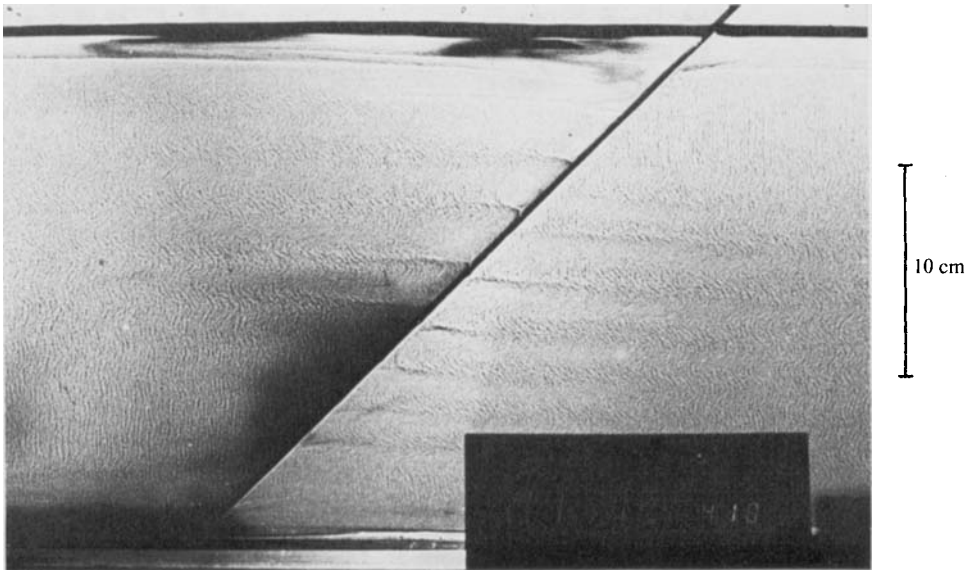

FIGURE 11. Layers formed by a sloping boundary in a finger stratification. In this case $G\rho = 0{\cdot}91$, $\theta = \frac{1}{4}\pi$ and the clock shows the time elapsed since the slope was inserted.

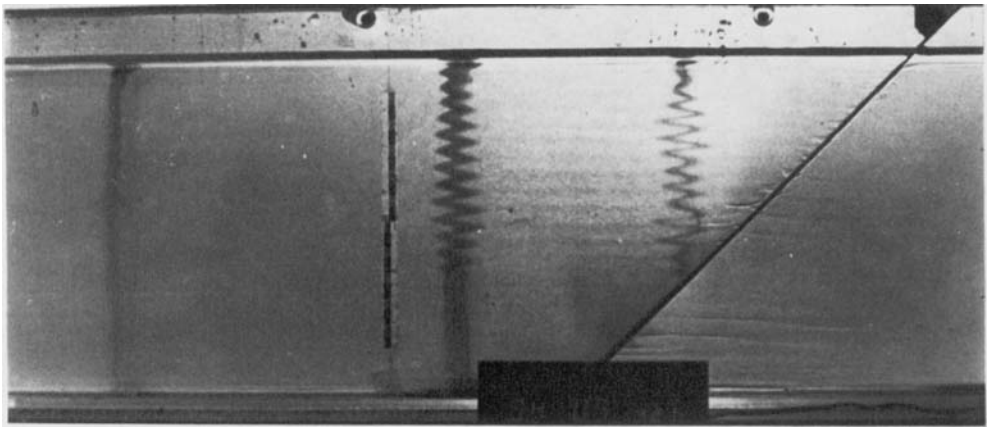

FIGURE 12. The large vertical shears and the finite vertical extent of the layers are seen from the distortions of these three vertical dye lines simultaneously put into the tank. In this run $G\rho = 0{\cdot}69$ and $\theta = \frac{1}{4}\pi$.

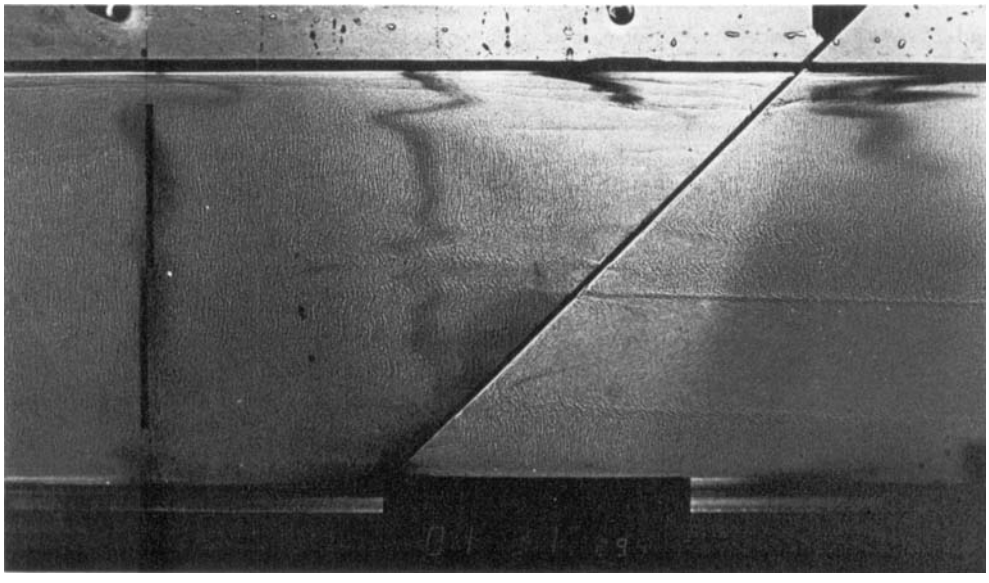

FIGURE 13. A large-scale layer formed by the slope flow in a finger stratification with $G\rho = 0{\cdot}97$ and $\theta = \frac{1}{4}\pi$.

was observed. This distortion increased in amplitude and eventually led to the breakdown of the fingers into a series of layers, separated by interfaces containing fingers. These interfaces extended right to the slope, thereby cutting off the slope flow, but the circulation in each individual layer was in the same sense as the original slope flow.

The fact that the circulation is in the same sense in each layer means that there are large shears across the interface. These shears are easily visualized by observing the distortion of vertical dye lines such as those shown on figure 12 (plate 4). In contrast to the diffusive case, the layers do not always reach the end walls of the tank. In figure 12 it can be seen that the magnitude of the shear decreases with increasing distance from the slope, with the dye line on the left showing almost no evidence of any layers. As this run developed in time the layers reduced in intensity and eventually weak finger motions re-established themselves over most of the tank, without any of the layers having reached the end walls of the tank.

A curious feature of these flows is that there were often large regions where no layers formed and the vertical motions of the fingers were undisturbed even quite close to the slope. Examples of these regions can be seen in the finger structure in figure 11 and in the lower part of the central dye streak in figure 12. These regions frequently remained undisturbed throughout an experiment and in the majority of cases exhibited the asymmetry of occurring near the bottom of the tank on the upper side of the slope and near the top of the tank on the underside.

At highly supercritical density ratios the breakdown of the finger structure into layers was observed to take a more dramatic form, an example of which is shown on figure 13 (plate 4). This figure shows the layering produced in a finger stratification with $G\rho = 0{\cdot}97$. As well as exhibiting layers of the form shown on figures 11 and 12, we see that there is a layer of much larger scale underneath the slope. This layer extends to the end wall of the tank (not visible in the photograph) and the motions inside the layer are extremely vigorous, as can be seen from the fact that the dye, visible above and below the layer, has been dispersed completely inside the layer itself. This form of layering was observed only for stratifications with an initial value of $G\rho > 0{\cdot}95$ and in every case the layer extended to the end wall of the tank. These layers are very reminiscent of those observed by Turner & Chen (1974) when a field of fingers at high $G\rho$ was disturbed mechanically (see figure 6 of their paper).

5. Discussion

There are many similarities, particularly in their gross properties, between diffusive and finger convection. One striking example is the fact that in both cases convection can occur when the fluid is stably stratified (the density increases with depth), and the net effect of the convection, when all the boundaries of the fluid are insulating, is to increase the magnitude of the mean vertical density gradient. Therefore, it is not very surprising that there are similarities between the motions produced in finger and diffusive stratifications by a sloping boundary. The experiments also revealed several differences between the two cases and so we begin this discussion with a qualitative comparison of the two situations. For the sake of convenience we consider only the upper side of the slope (figure 1).

The first observable response of both systems to the presence of the slope was the development of a flow near the slope. This flow was down the slope for the supercritical

finger stratifications, and either up the slope at low $G\rho$ or down the slope at high $G\rho$ in the diffusive case. The variation in direction of the diffusive slope flow is in general agreement with the theoretical prediction (2.12), although the precise details of the transition between the directions of the two flows was not checked experimentally. At high enough values of $G\rho$ fingers were formed locally near the slope. An examination of the theoretical vertical T and S gradients near the wall either for the initial diffusive response (2.10) and (2.11), or for the large time response (2.14) and (2.15) shows that in both cases the slope flow is not unstable to fingers, i.e. that we nowhere have $T_z < 0$ and $S_z > 0$, which is a necessary condition for fingers to occur. Thus the appearance of fingers must occur at an intermediate time when advection by the downslope flow reverses the vertical T and S gradients near the wall. Unfortunately, we are unable to write down the solution for this regime explicitly, but the fact that the large time solution always predicts an upslope flow implies that this was not realized in practice when $G\rho$ was large enough. Before this flow could develop, fingers formed which reinforced the downslope flow. Thus, at high enough $G\rho$, both systems have a downslope flow fed from above by fingers.

This general pattern continues for some time until horizontal motions develop which eventually produce horizontal layers. The layers are separated by relatively sharp interfaces which, in general, extend right to the slope. The slope flow is cut off into a series of cells with circulations in each layer in the same sense as the original slope flow. The interfaces contain fingers when the initial stratification is finger like, and a diffusive stratification breaks down into a series of diffusive interfaces.

It is a simple matter to see, in broad terms, how these layers arise. In § 2 we explained that the vertical density flux is different over the slope from its value in the interior of the fluid. Therefore horizontal density differences develop which can drive horizontal motions. However, the details of the breakdown of the slope flow are much less readily revealed. At high $G\rho$ the instability develops on a slope flow fed by fingers in both cases and appears to be a finite amplitude phenomenon. For low-$G\rho$ diffusive stratification the formation process seems to be connected with the sideways diffusive mechanism discussed by Thorpe *et al.* (1969) (see the appendix for details).

An obvious difference between the overall structure of the finger and diffusive layers is their horizontal extent. In the finger case the layers usually did not reach the end walls of the tank, but in the diffusive case, provided the slope flow was unstable to fingers, they always did. The reason for this different behaviour is not completely clear but it appears to be connected with the mechanism of the propagation of the layers from the slope into the interior. In the finger case this propagation takes place through the disruption of the fingers by the turbulent convective motions in the layer near the slope. The presence of the slope appears to be crucial to the continuation of this process as it provides, in each layer, a way to orient this convection into a net circulation.

In the diffusive case, on the other hand, the layers, once initiated, seem to be self-propagating with the slope playing only a minor role. This propagation is produced by the overturning associated with the nose, which is not found in the finger case, and which can release the energy stored in the unstably distributed component. The detailed behaviour of the nose is interesting and complicated. We restrict ourselves here to a couple of general points. As we see from the dye streaks on figure 4 (plate 2) a nose propagates into a stratified region which exhibits the familiar effects of upstream influence, which have produced velocity shears ahead of the nose. This

upstream influence is produced by waves propagating ahead of the nose. The speed of long waves Nh is considerably greater than the horizontal velocity of the nose: $U \sim 5 \times 10^{-3}$ (Nh) (see figure 10). The double-diffusive character of the flow is also evident from figure 10. As $G\rho$ increases the non-dimensional nose speed increases, as presumably there is more energy available in the stratification to drive the flow.

We have now discussed the obvious similarities and differences between the finger and diffusive stratifications. We conclude this section with some additional remarks on the details of the diffusive layers. Probably the most pressing question yet to be resolved in this context is that of the vertical scale of the layers. (The question also applies to the finger stratification but we have insufficient information to warrant discussing it in detail at this stage.)

In § 2 we mentioned that the layers which are formed by heating a stable salinity gradient laterally bear a strong resemblance to the diffusive case. In that situation the layer thickness scales with the length $\Delta T(dS/dz)^{-1}$, where ΔT is the horizontal temperature difference in density units and dS/dz the interior density gradient. The current situation is equivalent to imposing a fixed heat flux rather than a fixed temperature difference. Also, when fingers occur near the slope, it is extremely difficult to estimate the equivalent horizontal temperature difference, and so this simple scaling is not available.

When $G\rho$ is large enough for fingers to be produced by the slope flow ($G\rho > 0{\cdot}89$) the mean thickness of the layers $\bar{h}$ is proportional to $(1 - G\rho)^p$, where a least-squares fit to the data shows that $p = -0{\cdot}8 \pm 0{\cdot}1$ (figure 6). This increase in vertical scale as $G\rho \to 1$ reflects the fact that the vertical density gradient tends to zero in that limit.

It is interesting to note the similarity between this dependence on $G\rho$ and that found in an experiment where layers were formed sequentially in a double gradient diffusive stratification by imposing an unstable buoyancy flux at the top (Linden 1976). In the latter case it was found that the thickness of the first layer was proportional to $(1 - G\rho)^{-\frac{1}{2}}$. It was also shown in that case that as $G\rho \to 1$ the main contribution to the energy required to produce the layers came from the interior gradients, as is the case in these present experiments.

One final comment on the scale of the layers concerns the influence of the end walls of the tank. It has been observed previously (Turner & Chen 1974, figure 9*d*) that the vertical scale is different on opposite sides of the slope, and this may be due to the different distances to the end walls on either side of the slope. We also observed this difference in scales on one occasion but could find no systematic variation. We also found no systematic variation of layer scale with depth which might result from the variation in distance from the end walls to the slope. We have not, however, made a complete investigation of the effects of the finite dimensions of the container.

6. Conclusions

We have examined, both theoretically and experimentally, the motions induced in a fluid stratified with two components by the presence of an insulating sloping boundary. We find that the slope induces a flow along its length and that this flow can become unstable. As a result of this instability horizontal motions are produced which penetrate into the interior of the fluid. The stratification in the interior is altered by these motions and the final state consists of layers separated by relatively sharp interfaces.

The discovery that layers are formed when the basic stratification is finger like (i.e. the slower diffusing component is unstably distributed) opens up a new class of double-diffusive motions. Previous experiments with diffusive stratifications in the presence of a slope, and the equivalent case of heating a stable salinity gradient from the side, have revealed that layers were formed in those situations. It has been stated (Turner 1973) that the finger and diffusive types of convection are similar in the large, and the observations reported in this paper add another example of this similarity.

One of the reasons why this study was undertaken is that it seems to be one of the more simple ways of investigating some of the effects of horizontal inhomogeneities in the double-diffusive system. Even in this relatively simple case the experiments reveal a wide range of phenomena. We find that the scale of the layers depends on both the angle of the slope and the properties of the interior stratification. The horizontal extent of the layers also depends on the form of the interior stratification. Perhaps most striking of all are the relatively large velocities and vigorous convection driven by molecular processes in a stably stratified fluid merely through the presence of an insulating sloping boundary.

This work was carried out while J.E.W. was visiting DAMTP on a NATO Science Fellowship granted by the Royal Norwegian Council for Scientific and Industrial Research. Financial support was also provided by the British Admiralty. This work has benefited from discussion with Dr H. E. Huppert, who very generously allowed us access to his notes containing the time-dependent solutions given in § 2.

Appendix. Stability of the slope flow

The most amenable case for study is the low-$G\rho$ diffusive stratification. Here the slope flow is upwards at all times and perturbation of the long time solution reveals that the flow can become unstable, drawing its energy from the horizontal gradients of T and S in a manner similar to that described by Thorpe *et al.* (1969).

Consider the solutions (2.13)–(2.15). It is seen that the flow region may be separated into two parts: a boundary-layer region of thickness $\delta \sim M^{-1}$ in which the normal derivatives of the local T and S fields practically vanish, and an outer region defined by $\delta < \eta < l$, where

$$l = 2\{(1-\tau\lambda)\kappa_T t/(1-\lambda)\}^{\frac{1}{2}}, \tag{A 1}$$

representing a penetration depth of the transient T and S parts. Here the velocity essentially vanishes and $\partial T/\partial\eta$ and $\partial S/\partial\eta$ are approximately constant. Assuming now that $\delta \ll l$ and taking l to be 'frozen', we investigate the stability of the solutions in the outer region when subject to infinitesimal steady disturbances of the form $f(\eta)\exp(ik\xi)$, where k is a real wavenumber. We restrict ourselves to a situation with strong vertical stability such that the stratification forces the perturbations into thin, elongated cells. In this case we may neglect horizontal variations compared with vertical variations in the perturbation equations (see Hart 1971). We shall also assume that the slope is nearly vertical, i.e. that $\epsilon = \frac{1}{2}\pi - \theta$ is small. Essentially by applying Hart's arguments, we may, when δ is sufficiently small, obtain a first approximation by requiring that the perturbation stream function vanishes at $\eta = 0, l$. This finally leads to an eigenvalue equation

$$(1-\tau)^4\epsilon^2\lambda^2k^2R_S = 4k^6 + 4n^2\pi^2R_S, \quad n = 1, 2, \ldots, \tag{A 2}$$

where we have used the fact that $\lambda \ll \tau^{-1}$. The S-Rayleigh number in (A 2) is defined by $R_S = -g\gamma_S l^4/\nu\kappa_S$ and k has been non-dimensionalized by l^{-1}. The double-diffusive effect on the stability problem is obvious, since for $\tau = 1$, (A 2) has no solution for $R_S > 0$.

The analogy between this problem and the sideways-heated salinity gradient becomes clear if we introduce the horizontal T-difference ΔT_H associated with the imposed flux due to the tilting of the boundary. From (2.14) we obtain in our approximation

$$\Delta T_H = (1-\tau)\,\epsilon\gamma_T l. \tag{A 3}$$

An appropriate T-Rayleigh number may now be defined by

$$R_T = g\Delta T_H l^3/\nu\kappa_T = \epsilon\lambda\tau(1-\tau)\,R_S. \tag{A 4}$$

By substituting into (A 2), we find a critical Rayleigh number

$$R_T^c(\tau^{-1}-1) = 5{\cdot}9R_S^{\frac{3}{4}}, \tag{A 5}$$

for

$$k_c = 1{\cdot}3R_S^{\frac{1}{4}}, \tag{A 6}$$

which is formally identical to the marginal-stability criterion obtained by Thorpe *et al.* (1969) and Hart (1971) in the limit of large solute gradients.

The vertical scale of the problem is $h = \pi l/k$, since the slope is nearly vertical. Assuming that $R_T = R_T^c$, we find a layer thickness

$$h = \frac{\pi}{(1-\tau)\,\epsilon^{\frac{1}{4}}\lambda^{\frac{1}{4}}}\left(-\frac{12\,\nu\kappa_S}{g\gamma_S}\right)^{\frac{1}{4}}. \tag{A 7}$$

For the parameter regime we used, (A 7) implies that h is typically of order a few millimetres. A comparison with figure 2 is tempting, since we believe that our heuristic approach, at least qualitatively, reveals the physics of the problem. It must be stressed, however, that these experimental runs are outside the range of our asymptotic theory. In fact, to meet more rigorously the requirements implied by the analysis, quite a long time would have to elapse before instability manifested itself, and our assumption of a quasi-steady salt–sugar experiment could be violated.

REFERENCES

Chen, C. F. 1975 Double-diffusive convection in an inclined slot. *J. Fluid Mech.* **72**, 721–729.

Chen, C. F., Briggs, D. G. & Wirtz, R. A. 1971 Stability of thermal convection in a salinity gradient due to lateral heating. *Int. J. Heat Mass Transfer* **14**, 57–66.

Chen, C. F. & Wong, S. B. 1974 Double-diffusive convection along a sloping wall. *Bull. Am. Phys. Soc.* **19**, 1154.

Hart, J. E. 1971 On sideways diffusive instability. *J. Fluid Mech.* **49**, 279–288.

Linden, P. F. 1976 The formation and destruction of fine-structure by double-diffusive processes. *Deep-Sea Res.* **23**, 895–908.

Oster, G. 1965 Density gradients. *Scient. Am.* **213**, 70–76.

Phillips, O. M. 1970 On flows induced by diffusion in a stably stratified fluid. *Deep-Sea Res.* **17**, 435–443.

Thorpe, S. A., Hutt, P. K. & Soulsby, R. 1969 The effect of horizontal gradients on thermohaline convection. *J. Fluid Mech.* **38**, 375–400.

Turner, J. S. 1973 *Buoyancy Effects in Fluids.* Cambridge University Press.

Turner, J. S. & Chen, C. F. 1974 Two-dimensional effects in double-diffusive convection. *J. Fluid Mech.* **63**, 577–592.

Wunsch, C. 1970 On oceanic boundary mixing. *Deep-Sea Res.* **17**, 293–301.